Lab on a Chip

RSC Publishing

PAPER

View Article Online
View Journal | View Issue

Cite this: *Lab Chip*, 2013, **13**, 3755

Modulation of molecular hybridization and charge screening in a carbon nanotube network channel using the electrical pulse method†

Jun-Myung Woo,‡[a] Seok Hyang Kim,‡[a] Honnggu Chun,[b] Sung Jae Kim,[ac] Jinhong Ahn[a] and Young June Park*[a]

Received 26th April 2013,
Accepted 1st July 2013

DOI: 10.1039/c3lc50524c

www.rsc.org/loc

In this paper, we investigate the effect of electrical pulse bias on DNA hybridization events in a biosensor platform, using a Carbon Nanotube Network (CNN) and Gold Nano Particles (GNP) as an electrical channel. The scheme provides both hybridization rate enhancement of bio molecules, and electrical measurement in a transient state to avoid the charge screening effect, thereby significantly improving the sensitivity. As an example, the probe DNA molecules oscillate with pulse trains, resulting in the enhancement of DNA hybridization efficiency, and accordingly of the sensor performances in Tris–EDTA (TE) buffer solution, by as much as over three times, compared to the non-biasing conditions. More importantly, a wide dynamic range of 10^6 (target-DNA concentration from 5 pM to 5 μM) is achieved in human serum. In addition, the pulse biasing method enables one to obtain the conductance change, before the ions within the Electrical Double Layer (EDL) are redistributed, to avoid the charge screening effect, leading to an additional sensitivity enhancement.

Introduction

A biosensor is a device designed to detect or quantify a bio molecule, such as a particular DNA sequence or protein. In biomedical and forensic applications, the detection of bio molecules is critical, for quick and reliable diagnosis of disease, or genome analysis. Optical detection methods that use fluorescence labels,[1–5] or surface plasmon resonance,[6–10] have been widely used. But, in recent years, several attempts for electrical label-free detection have been made, to overcome the limitations of the optical method.[11–15] Among them, the electrical DNA biosensor, which can detect the change in electrical characteristics due to a DNA hybridization event, is a prospective alternative DNA detection method.[16–20] Electrical biosensors enable fast and inexpensive analysis with a direct electrical readout signal, and lead to the possibility of convergence and integration with other electrical devices.

The selectivity and sensitivity are critical issues limiting the biosensor performance.[21] The selectivity issue is related to the probe-target binding efficiency[22,23] and non-specific binding, in which non-target bio molecules stick to the probe layer, preventing target binding, or causing a false positive signal. Specifically, electrical biosensors are expected to respond only to the target analyte, and not to other similar molecules, called noisy molecules. However, an electrical biosensor cannot, in general, distinguish a probe-target binding signal from a probe-noisy molecule binding event. For example, the detection of low-abundant target molecules (under ng mL^{-1})[24,25] in human serum ($\sim$70 mg mL^{-1} in total protein content) is one of the greatest challenges in the biosensor field. On the other hand, the sensitivity issue is related to the limit of detection, and the signal-to-noise ratio.

In this paper, we apply an electrical pulse bias between the electrical channel, to which the probe molecules are attached, and the electrolyte, containing the target molecules, during the hybridization event. The method provides two important improvements: (i) enhancing the hybridization rate, and (ii) enabling transient signal detection, before the charge screening effect is resurrected. Firstly, the hybridization rates between the probe and target molecules are significantly improved, due to the mechanical oscillations of the probe and target molecules, caused by the external electric field around the charged probe molecules. Also, the dynamic motion of the probe molecules could suppress undesired binding events with nonspecific molecules since the motion largely enhances the desired binding events.

Secondly, it is possible to perform the transient measurement of the electrical channel current after pulse transition. By

[a]*Department of Electrical and Computer Engineering, Seoul National University, Seoul 151-744, Republic of Korea. E-mail: ypark@snu.ac.kr*
[b]*Department of Biomedical Engineering, Korea University, Horimkwan 116, Seoul 136-703, Republic of Korea*
[c]*Inter-university Semiconductor Research Center, Seoul National University, Seoul 151-744, Republic of Korea*

† Electronic supplementary information (ESI) available. See DOI: 10.1039/c3lc50524c

‡ These authors contributed equally.

properly choosing the timing of the measurement (within 1 μs) after single pulse transition, we can measure the electrical signal from the charges of the target molecule, before the charges are screened by the counter-ions in the bulk electrolyte. Generally, the real time monitoring of molecular hybridization events is performed under a buffer solution, where the Debye length is ~1 nm (comparable to 100 mM in ionic concentration), while the size of the biomolecule is over several nanometers. In this case, a large part of the charges from biomolecules is screened, and the sensitivity of the sensor is sacrificed. It takes a while for the counter-ions in the electrolyte system to redistribute, to reach a steady state for another screened state, after the pulse bias applied. The situation is quite similar to the deep depletion effect in a Charge Coupled Device (CCD),[26] in semiconductor engineering. Detection within the transient state can provide opportunities for sensitivity enhancement.

In summary of the proposition of the idea, we investigate the application of the 'pulse bias' method to electrical biosensors during molecular hybridization events. Both the hybridization events and charge screening events are modulated, and a significant enhancement of electrical biosensor performance in real time measurement is obtained.

Materials and methods

Device fabrication

All chemicals and solvents used in these experiments were of reagent grade, and used without further purification. The HPLC grade single-stranded DNA samples were purchased from Bioneer (Korea). The details are shown in Table 1. The purification and coating of SWCNT (ASP-100F (single wall) produced by Il-Jin Nanotech, Korea) were done as follows. SWCNTs exist in a form of bundles, due to the van der Waals attractive force. To disperse SWCNTs in an organic solvent, they should be pretreated with a liquid-phase oxidation (nitric acid treatment). The steps for dispersion recommended by the vendor of the SWCNTs were followed: the SWCNTs were ultrasonicated in nitric acid at 50 °C for 30 min, to purify and exfoliate from bundles. The SWCNTs were then neutralized with deionized (DI) water, and trapped on a membrane filter (Millipore, 0.2 μm pore size, 47 mm diameter), by the vacuum filtration method. The SWCNTs on the filter were dried in a vacuum oven chamber at 80 °C for 48 h. We used 1,2-dichlorobenzene (one of the widely used solvents for the dissolution of SWCNTs) to disperse SWCNTs, and then the ultrasonication process was performed again for 20 h.[27,28] The surface morphology of the sample was evaluated with an optical microscope, and field emission scanning electron microscopy (FE-SEM).

The test chips, having a concentric electrode structure, were fabricated at the Inter-university Semiconductor Research Center (ISRC) of Seoul National University, using a two-metal process, which consisted of aluminum as the first metal, and Au as the second metal. On a thermally oxidized Si wafer, the first metal routing patterns were formed, using conventional lithography and etching processes. Afterward, a 10 000 Å thick TEOS oxide film was deposited, and via contacts were formed. The substrate was evaporated, and patterned to form a 4000 Å concentric Au electrode, using the lift-off method. Using the CNT coating solution, the chips were coated with a CNT layer, by dipping them into the solution for 30 s, and then withdrawing them at a constant velocity of 3 mm min^{-1}. Thereafter, 1 nm thick GNPs were deposited on the CNN using a thermal evaporator, which resulted in the formation of a GNP layer on the CNN, by annealing at 250, 350 and 450 °C for 30 min. We mainly used GNPs annealed at 350 °C for the entire experiment.

DNA preparation

To immobilize the probe-DNA (p-DNA) molecules for the sensing of specific target molecules, bare CNN–GNP samples were immersed in 100 μM (10 μL) of p-DNA solution (Tris–EDTA buffer, pH 7.6) for 12 h at room temperature, and rinsed several times with TE buffer and deionized water. Human serum samples from human male AB plasma (H4522) were purchased from Sigma-Aldrich (Korea).

A Tektronix AFG3021 Pulse generator was used for the pulsed measurement. The electrical readout signal was measured by a Tektronix DPO7104 digital oscilloscope.

Results and discussion

To verify the idea, we use the unique biosensor architecture previously developed by our group.[29–31] We have reported a wide dynamic range DNA sensor based on CNN transistors, with GNP as a probe molecule docking place.[29] The sensor array platform used in this study consists of two gold (Au) electrodes with a concentric structure, CNN as an electrical channel, and GNP decorated on CNN for a molecule binding site, as shown in Fig. 1. The concentric electrode structure has been formed by the conventional two-metal process.[30] Each electrode is interconnected to each external electrical pad *via* the underlying aluminum metal layer. The channel consisting of the CNN and GNP can be fabricated by carbon nanotube dip-coating, and physical evaporation of Au, respectively.[29] The concentric electrode structure provides an interesting feature,

Table 1 DNA sequences used in this study

	ss-DNA	Sequences
Probe		5′-HSC6-C18-GCCATTCTCACCGGATTCAGTCGTC-3′
Target	Complementary	3′-CGGTAACACTGGCCTAGTCAGCAG-5′
	Noncomplementary	3′-GCCATTCTCACCGGATTCAGTCGTC-5′

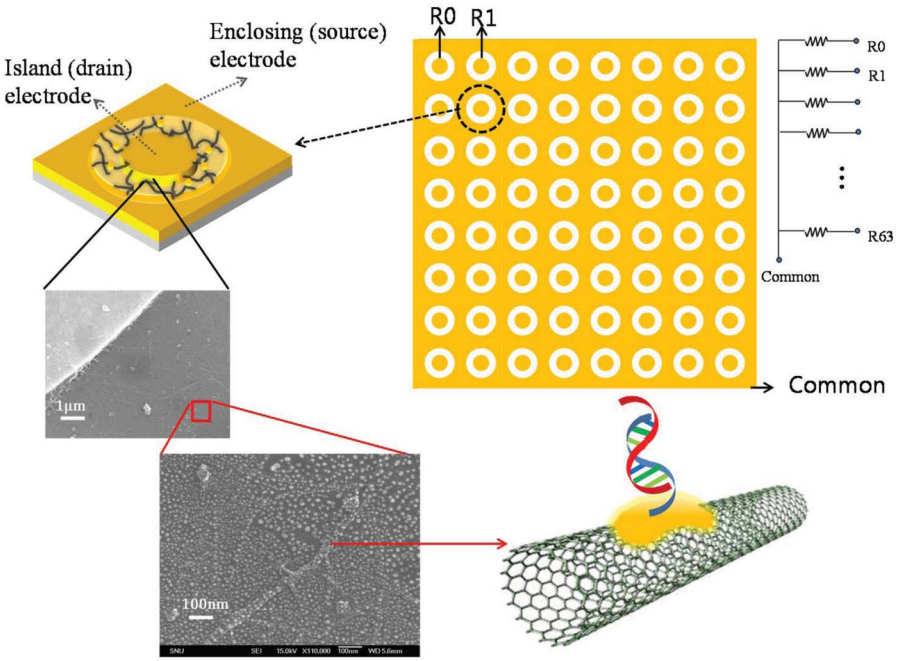

Fig. 1 Conceptual diagram of sensor array, and structure of individual sensor device. The CNN with Gold Nano Particles (GNP) is integrated between the concentric electrodes. Thiolated probe DNA is immobilized on Au nano-islands, and bound with complementary t-DNA.

called the ''self-gating effect''.[30,31] The effect can be elaborated as the electrical potential of an electrolyte solution applied on the sensor platform being generally determined by the potential of the enclosing (source) electrode, which has much larger area, due to the capacitance ratio (1000 : 1 in this work). Applying the drain bias to the island (drain) electrode, the conductance of the CNN channel between two electrodes can be modulated by the electrolyte gating, resulting from the preset bias value at the enclosing electrode. In other words, the electrolyte gating effect can be obtained in our sensor array platform, without any external gate electrode (see ESI,† for details of the self-gating effect).

For an application of this sensor array to DNA sensing, thiolated 25-mer probe ssDNA (p-DNA) molecules (approximately 50 nm) are immobilized on the Au islands, as shown in Fig. 1. The immobilization of p-DNA was by treatment at room temperature overnight. The immobilized p-DNA samples were washed with TE buffer solution, for removal of non-specific bound molecules.

It should be emphasized here that an alternating electrical field can easily be applied between the p-DNA molecules and the electrolyte, thanks to the electrode structure shown in Fig. 1, since the electrical potential of a bulk electrolyte is relatively stable.

The schematics of the pulse voltage train applied to the drain electrode (island) as V_{in}, during the hybridization events between the p-DNA and target-DNA (t-DNA), are shown in Fig. 2 (a) and (b). Though one could apply various types of AC biasing, such as wave, triangle and saw-tooth, we have used the step profile only, because it can tell the steady-state current value, while other types of profile do not have an inherently steady state. The time dependent voltage of an operational amplifier, V_{out}, which reflects the current through the CNN channel, can be divided into two regions. The 1st region is the transient state, when the ionic charges in the electrolyte double layer are redistributed.[32,33] In the 2nd region, after the steady state is reached, the conductance is changed, solely due to the enhancement of the hybridization rate, which will be elaborated as follows.

As the t-DNA hybridizes with p-DNA immobilized on the GNPs, we can quantify and define the sensitivity, as the change of the CNN channel conductance, from the change of the amplifier's output voltage. The change in the electrical current of the CNN–GNP system after the hybridization event can be explained by the work function change of the GNP, thereby modulating the CNN conductance.[29] The DNA motion by the pulse biasing during the hybridization is shown schematically in Fig. 2 (c). When positive bias is applied to the CNN channel *via* the drain electrode, the immobilized p-DNA molecules with negative charges are attracted to the CNN surface (left image of Fig. 2 (c)), while they stretch during the negative bias (right image of Fig. 2 (c)). Thus, the dynamic motion of DNA in the electrolyte solution, induced by the pulse bias, contributes to the enhancement of the hybridization efficiency. The increase of the hybridization rate constant (k_h) leads to not only faster hybridization with t-DNA, but an increase in the number of dsDNA, after the hybridization reaches saturation.

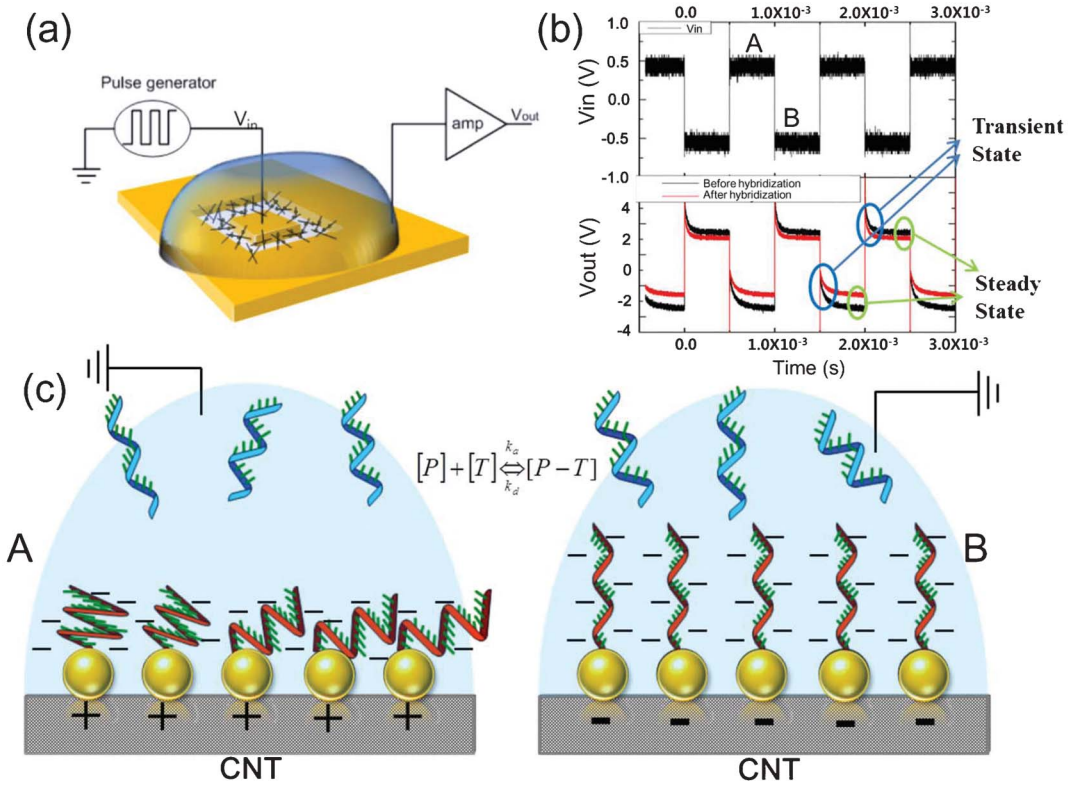

Fig. 2 Scheme of the pulse biasing method: (a) configuration for pulse biasing in the sensor device, (b) applied input bias and output, and (c) schematic illustration of the p-DNA motion by pulse biasing (positive and negative) during hybridization.

After the TE buffer containing complementary t-DNA is applied to the sensor array device, the pulse bias at various frequencies is applied to a specific sensor device, with the other devices remaining unbiased, for comparison. The electric potential applied to the island electrode is in the range from −0.5 V to +0.5 V, where the electrode oxidation–reduction reaction with ions hardly occurs.[34] Also, the conductivities of electrolyte (NaCl: 10 mM) and CNN are O(10^{-3}) S cm^{-1}, O(10) S cm^{-1}, respectively.[35,36] Thus, the unwanted current between the island electrode and the enclosing electrode can be neglected, compared with the channel current.

Enhancement of sensitivity using a pulse train

Fig. 3 (a) shows the sensitivity enhancement as a function of pulse frequency (±0.5 V in amplitude and 10 Hz, 100 Hz, 1 kHz, 10 kHz, 100 kHz in frequency). The sensitivity data less than 10 Hz was almost the same as the case for DC bias, and the frequency over 100 kHz may not be appropriate, since the measurement should be performed within the RC time constant of the whole system (O(1) micro-seconds). Notice that we need to measure the current after the steady state is reached in pulse duration during the hybridization event, in order to see the pure effect on the hybridization event. In this sense, there should be an optimum frequency value for maximizing binding efficiency, which is likely to be a function of DNA length. In our case, frequency near 1 kHz turns out to give the maximum sensitivity, as shown in Fig. 3 (a).

Fig. 3 (b) shows the conductance change as the function of time, after applying the TE buffer with the complementary t-DNA of 5 μM. Compared with the devices without bias (DC biasing in 0.3 V only during measurement), the pulse biasing schemes show higher sensitivity and faster response, for both 0.5 V and −0.5 V, in ±0.5 V pulses. As shown in the inset of Fig. 3 (b), V_{out} (red line) sharply changed, and reached a steady state within a short time period, depending on V_{in} (black line). The normalized currents were measured at the steady state, as denoted with arrows. The time constants from the exponential fitting with the measurement data are about 460 s, and 80 s for the DC and pulsed schemes, respectively. It is interesting to note that the sensitivity in the positive pulse response is higher, than that in the negative pulse response. We consider that the negative charged dsDNAs on the GNP become closer to the CNN channel by an electrical attraction in the positive bias, thereby showing higher sensitivity, which is hereafter defined as the normalized conductance change by the hybridization event. After the DNA hybridization for 800 s, the sensitivity of the sensor device that has undergone pulse biasing is −38% (blue triangle in Fig. 3 (b)), while the sensitivity of the others (*i.e.* unbiased devices) is −10% (±4%), for 5 μM complementary t-DNA (purple square). The hybridization rate constants k_h for the DC and pulsed scheme are estimated to be 0.66 and 2.47 (10^3 M^{-1} s^{-1}), respectively, by the time constant extracted from the real time measure-

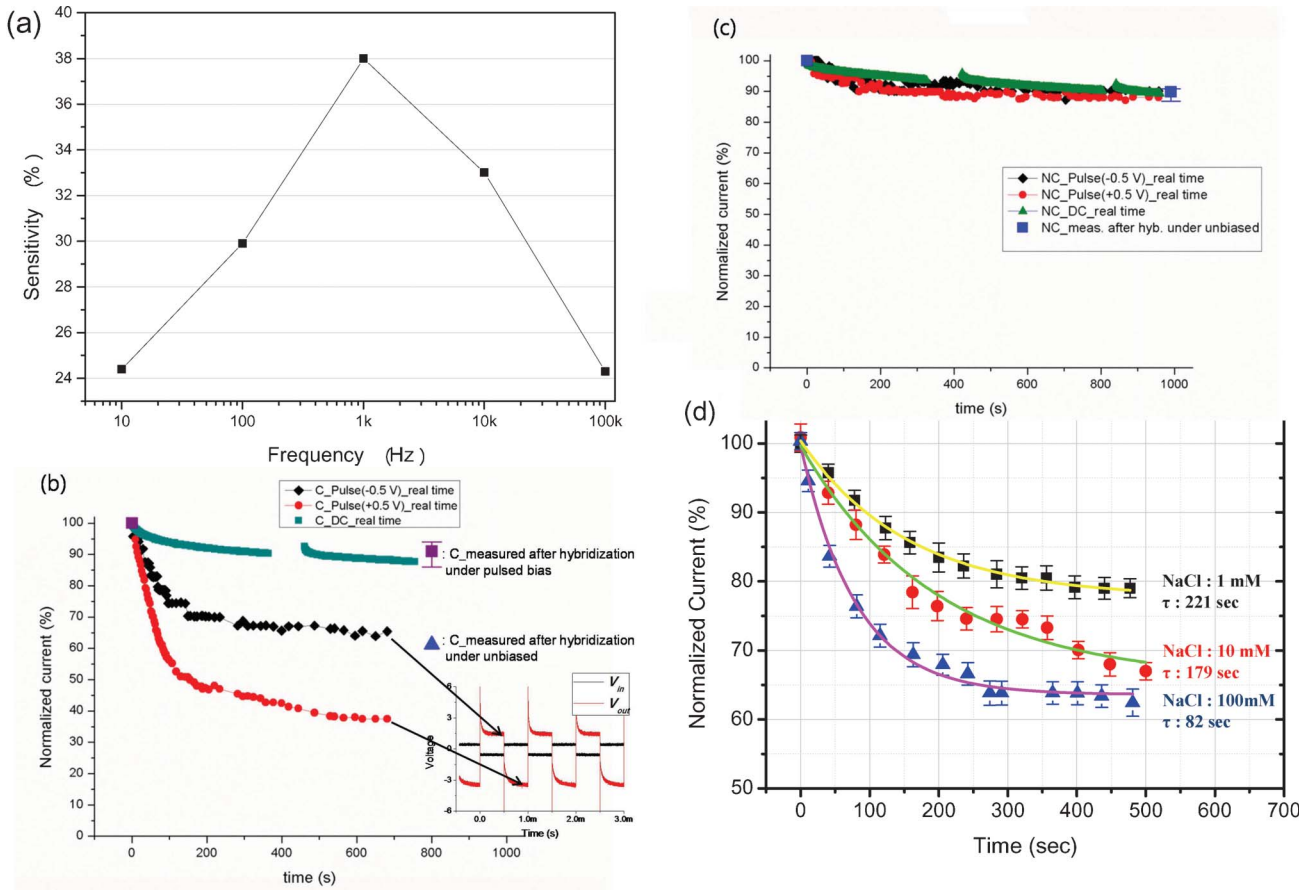

Fig. 3 (a) Sensitivity data for 5 different frequencies of the pulsed bias signal applied during hybridization with the complementary t-DNA. The pulse is of ±0.5 V in amplitude, and 10 Hz, 100 Hz, 1 kHz, 10 kHz, 100 kHz in frequency. Real time measurement during DNA hybridization of (b) complementary t-DNA, and (c) non-complementary (NC) t-DNA, in TE buffer solution. (b) Pulse biasing is applied to the specific device, while the other devices are left without biasing, during complementary hybridization. The pulse biased device is measured in real time. After considerable hybridization time, we measured the conductance change of every device, by DNA hybridization. Real time data for the DC conditions is from our previous work.[15] (c) Pulse biasing is applied to the specific device, while other devices are left without biasing, during NC hybridization. In the same manner, the real time measurement in the specific device, and conductance change by NC hybridization in every device, are plotted. (d) The effect of concentration of electrolyte. Real-time conductance change during DNA hybridization for various salt concentrations (NaCl: 1 mM, 10 mM and 100 mM).

ment data. Due to the pulse biasing, DNA hybridization efficiency is prominently improved, leading to a faster response, and a better sensitivity.

Similar data for the TE buffer containing the non-complementary (NC) t-DNA of 5 μM are plotted in Fig. 3 (c). During the hybridization event for 1000 s, both the pulsed bias (±0.5 V at 1 kHz) and the DC bias were applied, and then the final currents were measured under the DC conditions. Compared to these control experiments, the case of complementary DNA hybridization under the pulse biased conditions showed outstanding improvements in the sensitivity, in comparison with Fig. 3 (b). It is interesting to notice that there is no significant difference in sensitivity between the devices undergoing the pulse bias (−11%), and the devices without bias (−12% ± 3%), during the hybridization, unlike the case of complementary t-DNA. (By this observation, we can conclude that this reaction is "a diffusion-limited reaction". The reaction can be enhanced by a mechanical oscillation (or agitation) to improve the collision frequency of two molecules.[37] This fact supports our enhancement scheme by AC biasing). Undesirable current change in this control experiment could be explained by the non-specific interaction between the NC t-DNA and the CNN channel. The interaction gives rise to an effect of doping the CNT by the negatively charged DNAs, so that the current decreases.[38] Also, non-specifically adsorbed t-DNA between the CNN channel and electrodes increases the Schottky barrier, by modulating the metal workfunction,[39] thereby reducing the p-type conduction, due to changes in the CNT–metal work function difference. Compared to these reductions, however, the complementary hybridization gives a salient contribution to the current modulation, as shown in Fig. 3 (b).

The salt concentration of buffer solution is adjusted with NaCl giving final concentrations from 1 mM to 100 mM. The pulse voltage with 0.5 V amplitude and 1 kHz frequency is applied to the drain electrode during the DNA hybridization. Fig. 3 (d) shows the real time measurement data during the DNA hybridization. All sensor devices initially contain the

complementary t-DNA of 5 μM concentration for each buffer concentration of 1 mM, 10 mM and 100 mM. Compared with the device with the t-DNA in diluted buffer solution conditions (1 mM and 10 mM), the sensitivity and response time with the t-DNA in 1× buffer solution (~100 mM) shows improvement. After 500 s in DNA hybridization, the conductance of the device in 1× buffer solution decreases by 37%, while the conductance of the device in diluted buffer solution decreases by approximately 33% (NaCl: 10 mM), 23% (NaCl: 1 mM). We have estimated the time constants from the exponential fitting of real time hybridization measurements for both 1× buffer solution and diluted buffer solutions, leading 82 s for 1× buffer, 179 s (NaCl: 10 mM) and 221 s (NaCl: 1 mM). The trend of results is due to screening of electrostatic penalties (lower electrolyte concentration → longer screening length → preventing the binding between probe and target) to hybridization at lower ionic strengths.[40,41]

In summary, remarkable sensitivity, which is about 3.8 times higher than the unbiased conditions, is obtained for real time measurements of DNA hybridization using the pulse bias scheme, with reasonable selectivity.

Enhancement of dynamic ranges in human serum

DNA sensors for quick and reliable detection of diseases, *i.e.* point-of-care-testing (POCT), frequently require the real time detection of t-DNA in human serum without the washing step, which is generally needed to remove the non-specific binding with noisy molecules that are contained in human serum.[42,43] We applied the pulse bias scheme to detection of the complementary DNA hybridization of a wide range of concentrations in the human serum conditions. Fig. 4 shows the conductance change, as the function of the concentration of complementary t-DNA in human serum. The sensitivity data are taken at 20 min, after applying the t-DNA in serum. In Fig. 4, it is striking to observe that the sensor device with the pulsed bias during hybridizations gives a distinct signal in sensitivity, while the control device without pulsed bias does not show any sensitivity, other than noise signal. The sensitivity matches well with the Langmuir equation

$$\frac{\Gamma}{\Gamma_{max}} = \frac{(K_a c)^{\alpha}}{1+(K_a c)^{\alpha}}, \quad (1)$$

with fitting parameters $K_a = 6.08 \times 10^8$ and $\alpha = 0.22$, where K_a is an equilibrium constant, c is the concentration of complementary t-DNA, and α is the pseudo-Gaussian distribution of binding energy of set width.[44] In addition, the new scheme achieves a signal-to-noise ratio (SNR) of 6.6 in the detection at 5 pM t-DNA concentration, even in the serum conditions. At each measured concentration point from 5 pM to 5 μM, the SNR is estimated to be 6.6–15 (see ESI,† for comparison to the literature).

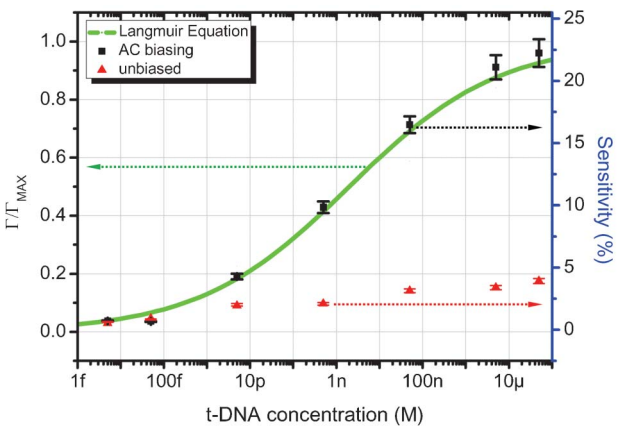

Fig. 4 Sensitivity of the electrical DNA sensor *vs.* t-DNA concentration, for two groups of sensor devices after hybridization with t-DNA in the serum conditions; one group hybridized under the pulsed bias (±0.5 V in amplitude and 1 kHz in frequency), and the other group hybridized under the unbiased conditions. The pulse biasing during hybridization achieves remarkable improvement in sensitivity.

Effect of GNP size

In order to see how the LOD (Limit of Detection) of the device was affected by the GNP sizes, devices with different GNP sizes (*i.e.* with different annealing temperature) were prepared for DNA hybridization experiments. Fig. 5 (a) shows SEM images of the GNPs before, and after, the annealing process. The average diameter of the GNP on the SWCNT network deposited using the thermal evaporator deposition method was originally 8.98 ± 0.31 nm before annealing, but its size increased to 11–13 nm, after annealing at different temperatures. The average diameter of GNP sizes as a result of annealing at 250, 350 and 450 °C were measured to be 11.97 ± 0.76, 13.09 ± 0.69 and 13.67 ± 0.52 nm, respectively, as shown in Fig. 5 (b). Fig. 5 (c) shows the data as in Fig. 4 (for the device with GNP annealed at 350 °C), but with various GNP sizes. Based on the result of the experiment, it was observed that there was no significant difference in the LOD and dynamic range, compared to the device without any additional annealing treatments (*i.e.* device with smaller GNP size), as shown in Fig. 5 (c).

Transient measurement using a single step pulse

Now, we consider additional sensitivity enhancement from our pulsed bias measurement platform, which is called transient measurement. In transient measurement, the channel current is measured before the ions in the EDL are redistributed, *i.e.* avoiding the charge screening effect. Fig. 6 describes the schematic mechanism of the sensitivity enhancement on the transient state, after single step pulse bias. After the pulse transition, the counter-ions surrounding the charged target molecule in the initial state (A) are swept away by the electric field in the extended EDL during the transient state (C), and finally reach a new steady state (D). During the transient state, charged molecules (dsDNA) can influence the CNN channel. It should be noticed that the scheme would be applied to sensor devices after the completion of the hybridization and/or during the DNA hybridization under the pulsed bias conditions, because in our platform, the channel current is constantly monitored during the hybridization event.

In our previous modeling study,[32,33] we verified the feasibility of the sensitivity enhancement, by solving the equations for the charge distribution and the motion of ions

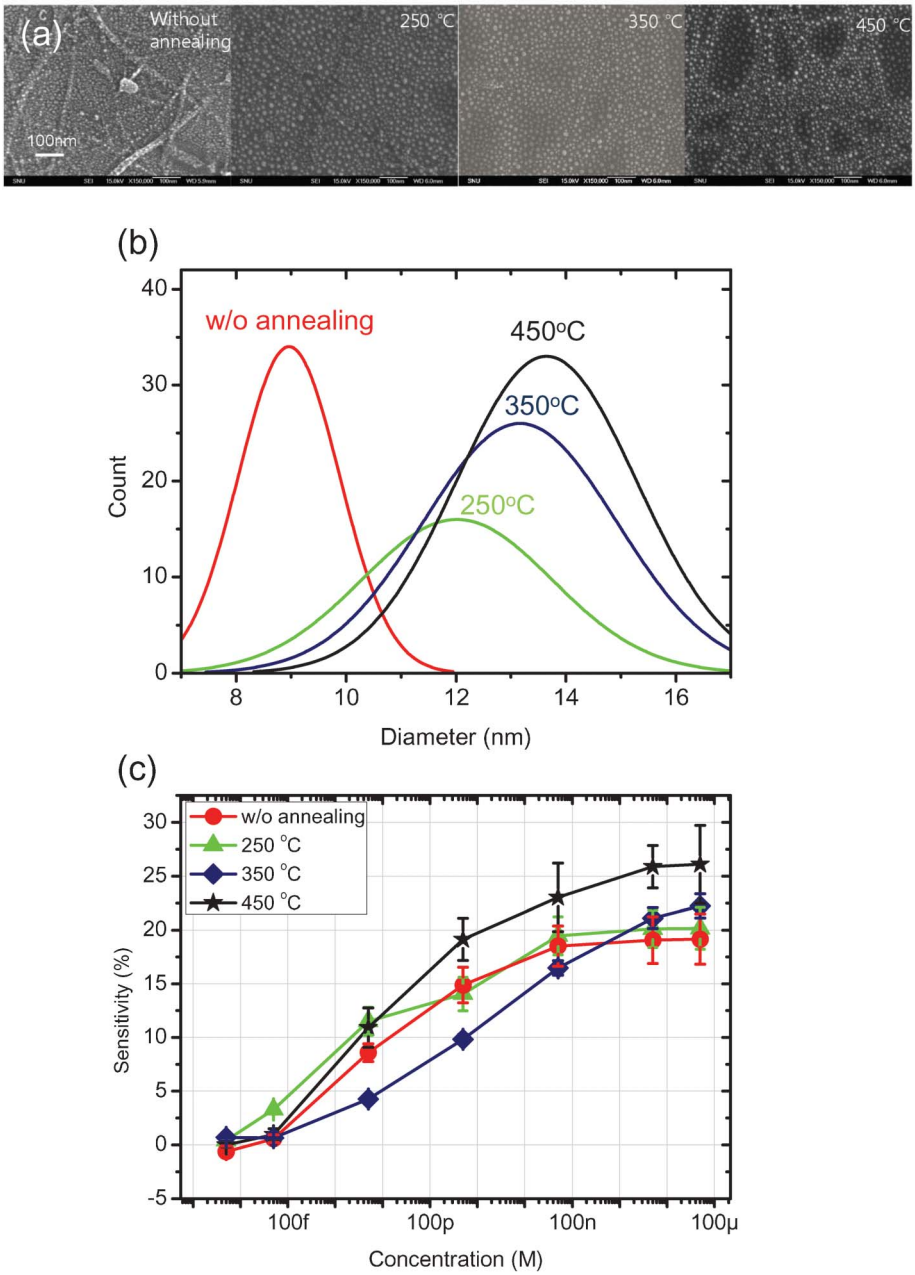

Fig. 5 (a) SEM images, and (b) size variation of GNP, as a function of annealing temperature from 250 °C to 450 °C. About 50 GNP diameters for each device were randomly measured (w/o annealing: 8.98 nm, 250 °C: 11.97 nm, 350 °C: 13.09 nm, 450 °C: 13.67 nm). (c) The LODs of DNA hybridization as a function of annealing temperature. Each measurement was done more than 5 times, with 5 different devices.

in the buffer solution (see ESI,† for details of the calculation). Fig. 7 shows the sensitivity *via* the time, measured using the transient measurements for two device samples, after a hybridization of 1000 s; one hybridized under the pulsed bias conditions (red line), the other under the unbiased conditions (black line). For the device sample hybridized under AC biasing, a pulsed bias with ± 0.5 V in amplitude and 1 kHz in frequency has been applied. In our measurement system, the output current from the operational amplifier includes the capacitive current through the electrolyte system,[45] and is subtracted, to obtain the intrinsic channel current. Sensitivity is defined as the ratio of change in the channel currents before and after hybridization to the initial current before hybridization. As can be seen in Fig. 7, the sensitivity is maximized at around 1 μs for both sensor devices, as predicted in previous numerical works.[32,33] The sensitivity is enhanced from 7% (steady state sensitivity) to 40% (maximum transient sensitivity), and from 38% to 75%, for the samples undergoing the unbiased, and AC hybridization, respectively. Considering the short Debye length (about 1 nm), the sensitivity value from the steady state measurement is surprisingly large, for the sample undergoing the AC hybridization (38%), compared with 7% of

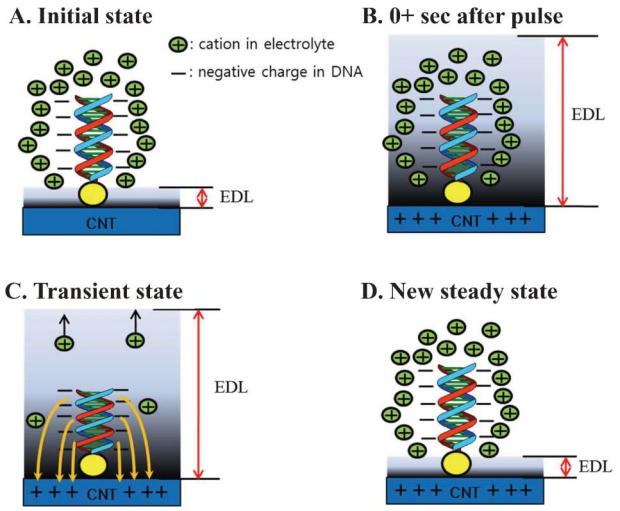

Fig. 6 Conceptual scheme for the transient measurement, after the unit step pulse bias is applied between the CNT channel and the electrolyte solution.

the sample undergoing the unbiased hybridization. The mechanism of current modulation due to hybridization density on the Au nanoparticles of our sensor platform should be a subject of future theoretical study.

Conclusion

In summary, a new pulse bias scheme has been proposed, and an enhancement in the sensor performance has been obtained, for the detection of DNA hybridization events. The mechanisms for the improvement have been elucidated by the oscillating motion of the negatively charged probe DNA with the pulsed bias. Thereby, the hybridization rate constant k_h is ~3 times enhanced, compared to the unbiased conditions. However, theoretical studies should be performed, in terms of a relationship between the hybridization rate and the mechanical motion of the probe molecules; which, in turn, is a function of the shape and frequency of the pulse trains, not to mention a function of the size and mass of the probe molecules. It has been shown that an LOD of as low as ~5 pM concentration can be achieved, in the detection of DNA in the human serum conditions. Also, by transient measurement after the step pulse, additional sensitivity enhancement is achieved, due to the removal of the charge screening effect. Therefore, the new scheme could be extended to a general affinity-based biosensor, where charged probe molecules are immobilized.

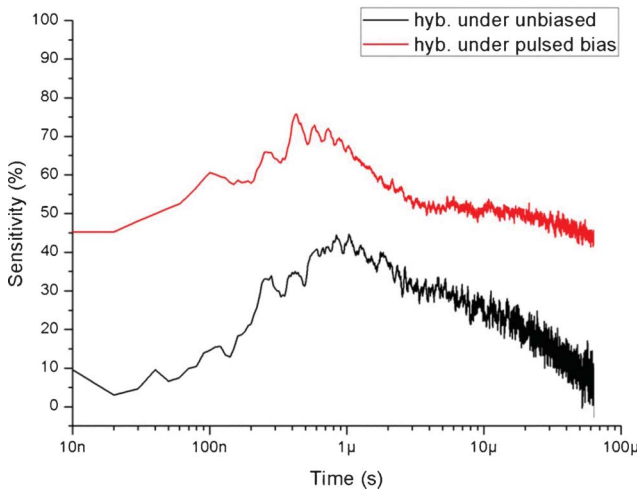

Fig. 7 Sensitivity *vs.* time after the unit pulse is applied (transient measurement), for two sensor devices, after hybridization of 1000 s. The data denoted by the black line and by the red line are for the devices hybridized with the complementary t-DNA of 5 μM, under the unbiased conditions, and AC bias conditions, respectively. The measurements were conducted in TE buffer solution.

Acknowledgements

This work was supported by the Center for Integrated Smart Sensors funded by the Ministry of Science, ICT & Future Planning as Global Frontier Project (CISS-2012054186); and by the R&D Program of MKE/KEIT [10033590], Development of Disposable Cancer Diagnosis Sensor of Home-care Type with High Sensitivity; and by the Pioneer Research Center Program through the National Research Foundation of Korea funded by the Ministry of Science, ICT & Future Planning (NRF-2012-0009555). S. J. Kim was supported by Future-based Technology Development Program (Nano Fields) (2009-0082952) through the National Research Foundation of Korea (NRF) funded by the Ministry of Science, ICT & Future Planning.

References

1 M. S. T. Gonçalves, *Chem. Rev.*, 2009, **109**, 190–212.
2 J. Yuan and G. Wang, *J. Fluoresc.*, 2005, **15**, 559–568.
3 M. Takahashi, K. Nokihara and H. Mihara, *Chem. Biol.*, 2003, **10**, 53–60.
4 H.-J. van Manen and C. Otto, *Nano Lett.*, 2007, **7**, 1631–1636.
5 J. Seelig, K. Leslie, A. Renn, S. Kühn, V. Jacobsen, M. van de Corput, C. Wyman and V. Sandoghdar, *Nano Lett.*, 2007, **7**, 685–689.
6 J. Homola, S. S. Yee and G. Gauglitz, *Sens. Actuators, B*, 1999, **54**, 3–15.
7 P. K. Jain and M. A. El-Sayed, *J. Phys. Chem. C*, 2007, **111**, 17451–17454.
8 M. Caldow, S. L. Stead, J. Day, M. Sharman, C. Situ and C. Elliott, *J. Agric. Food Chem.*, 2005, **53**, 7367–7370.
9 E. Fujii, T. Koike, K. Nakamura, S. Sasaki, K. Kurihara, D. Citterio, Y. Iwasaki, O. Niwa and K. Suzuki, *Anal. Chem.*, 2002, **74**, 6106–6110.
10 O. R. Bolduc, J. N. Pelletier and J.-F. Masson, *Anal. Chem.*, 2010, **82**, 3699–3706.
11 M. Dhayal and D. M. Ratner, *Langmuir*, 2009, **25**, 2181–2187.

12 I. H. El-Sayed, X. Huang and M. El-Sayed, *Nano Lett.*, 2005, **5**, 829–834.
13 B. R. Baker, R. Y. Lai, M. S. Wood, E. H. Doctor, A. J. Heeger and K. W. Plaxco, *J. Am. Chem. Soc.*, 2006, **128**, 3138–3139.
14 F. Vollmer and S. Arnold, *Nat. Methods*, 2008, **5**, 591–596.
15 K. Maehasi, T. Katsura, K. Kerman, Y. Takamura, K. Matsumoto and E. Tamiya, *Anal. Chem.*, 2007, **79**, 782–787.
16 G. Libo, H. Jinghong, Z. Hong and C. Xiang, *Proc. SPIE*, 2001, **4414**, 47–49.
17 F. Wei, B. Sun, Y. Guo and X. S. Zhao, *Biosens. Bioelectron.*, 2003, **18**, 1157–1163.
18 D.-S. Kim, Y.-T. Jeong, H.-K. Lyu, H.-J. Park, J.-K. Shin, P. Choi, J.-H. Lee and G. Lim, *Biosens. Bioelectron.*, 2004, **20**, 69–74.
19 H. Berney, J. West, E. Haefele, J. Alderman, W. Lane and J. K. Collins, *Sens. Actuators, B*, 2000, **68**, 100–108.
20 F. Pouthas, C. Gentil, D. Cote and U. Bockelmann, *Appl. Phys. Lett.*, 2004, **84**, 1594–1596.
21 J. S. Daniels and N. Pourmand, *Electroanalysis*, 2007, **19**, 1239–1257.
22 G. Bhanot, Y. Louzoun, J. Zhu and C. DeLisi, *Biophys. J.*, 2003, **84**, 124–135.
23 S. Sorgenfrei, C. Chiu, R. L. Gonzalez Jr, Y.-J. Yu, P. Kim, C. Nuckolls and K. L. Shepard, *Nat. Nanotechnol.*, 2011, **6**, 126–132.
24 I. M. Thompson, D. K. Pauler, P. J. Goodman, C. M. Tangen, M. S. Lucia, H. L. Parnes, L. M. Minasian, L. G. Ford, S. M. Lippman, E. D. Crawford, J. J. Crowley and C. A. Coltman Jr, *N. Engl. J. Med.*, 2004, **350**, 2239–2246.
25 L. Maattanen, A. Auvinen, U. H. Stenman, T. Tammela, S. Rannikko, J. Aro, H. Juusela and M. Hakama, *J. Natl. Cancer Inst.*, 2001, **93**, 552–553.
26 I. M. Baker, J. D. E. Beynon and M. A. Copeland, *Electron. Lett.*, 1973, **9**, 48–49.
27 M. Yang, D.-H. Kim, W.-S. Kim, T. J. Kang, B. Y. Lee, S. Hong, Y. H. Kim and S.-H. Hong, *Nanotechnology*, 2010, **21**, 215501.
28 E. Y. Jang, T. J. Kang, H. W. Im, D. W. Kim and Y. H. Kim, *Small*, 2008, **4**, 2255–2261.
29 J. W. Ko, J.-M. Woo, J. Ahn, J. H. Cheon, J. H. Lim, S. H. Kim, H. Chun, E. Kim and Y. J. Park, *ACS Nano*, 2011, **5**, 4365–4372.
30 J. H. Cheon, J. Lim, S. M. Seo, J.-M. Woo, S. H. Kim, Y. Kwon, J. W. Ko, T. J. Kang, Y. H. Kim and Y. J. Park, *IEEE Trans. Electron Devices*, 2010, **57**, 2684–2689.
31 D. W. Kim, G. S. Choe, S. M. Seo, J. H. Cheon, H. Kim, J. W. Ko, I. Y. Chung and Y. J. Park, *Appl. Phys. Lett.*, 2008, **93**, 243115(1–3).
32 J.-M. Woo, S. H. Kim and Y. J. Park, *IEEE Int. Workshop on Compact Modeling*, 2011.
33 J.-M. Woo, S. H. Kim and Y. J. Park, *IEEE SISPAD*, 2012, 177–180.
34 R. G. Pearson, *J. Am. Chem. Soc.*, 1986, **108**, 6109–6114.
35 B. J. Hinds, N. Chopra, T. Rantell, R. Andrews, V. Gavalas and L. G. Bachas, *Science*, 2004, **303**, 62–65.
36 T. W. Ebbesen, H. J. Lezec, H. Hiura, J. W. Bennett, H. F. Ghaemi and T. Thio, *Nature*, 1996, **382**, 54–56.
37 A. Fersht, in *Enzyme structure and mechanism*, W. H. Freeman and Company, 2nd edn, 1985, ch. 4, pp. 147–148.
38 A. B. Artyukhin, M. Stadermann, R. W. Friddle, P. Stroeve, O. Bakajin and A. Noy, *Nano Lett.*, 2006, **6**, 2080–2085.
39 S. Heinze, J. Tersoff, R. Martel, V. Derycke, J. Appenzeller and Ph. Avouris, *Phys. Rev. Lett.*, 2002, **89**, 106801(1–4).
40 J. Fuchs, J.-B. Fiche, A. Buhot, R. Calemczuk and T. Livache, *Biophys. J.*, 2010, **99**, 1886–1895.
41 D. Irving, P. Gong and R. Levicky, *J. Phys. Chem. B*, 2010, **114**, 7631–7640.
42 A. J. Haes and R. P. Van Duyne, *J. Am. Chem. Soc.*, 2002, **124**, 10596–10604.
43 Y. Xiao, A. A. Lubin, A. J. Heeger and K. W. Plaxco, *Angew. Chem.*, 2005, **117**, 5592–5595.
44 A. W. Peterson, L. K. Wolf and R. M. Georgiadis, *J. Am. Chem. Soc.*, 2002, **124**, 14601–14607.
45 J.-M. Woo, PhD thesis, Seoul National University, 2012.